A Raman-delayed nonlinearity for elliptically polarized ultrashort optical pulses

Alexandre Stathopulos, Stefan Skupin, Luc Bergé

A Raman-delayed nonlinearity for elliptically-polarized ultrashort optical pulses

Alexandre Stathopulos[1,2*], Stefan Skupin[3] and Luc Bergé[1,2]

[1*]CEA, DAM, DIF, Arpajon, 91297 Arpajon, France.
[2]Université Paris-Saclay, CEA, LMCE, Bruyères-le-Châtel, 91680, France.
[3]Institut Lumiére Matiére, UMR 5306 Université Lyon 1-CNRS, Université de Lyon, Villeurbanne, 69622, France.

*Corresponding author(s). E-mail(s): alexandre.stathopulos@cea.fr;

Abstract

We address the role of the delayed Kerr nonlinearity associated with stimulated rotational Raman scattering on the propagation of intense ultrashort two-color filaments with elliptical polarization in gases and examine its impact on the generation of optical frequencies as well as terahertz frequencies. We find that in air the nonlinearity associated with stimulated Raman scattering strongly impacts the dynamics of the laser filaments and modifies the overall pulse spectral content. In particular, it alters the THz spectra upon propagation in the filamentation regime. Differences between linearly and circularly polarized two-color pump pulses are discussed.

Keywords: nonlinear optics, ultrashort laser pulses, terahertz pulse generation

1 Introduction

The propagation of femtosecond, intense laser pulses in air has important applications for active or passive remote sensing, ultrafast Lidar or artificial lightning. Ultrashort laser pulses with high enough peak power undergo unique interactions with the atmosphere in which both linear and nonlinear mechanisms play a key role. In particular, laser filaments produced by ultrashort light pulses proceed from the dynamic balance between Kerr self-focusing and plasma defocusing [1–3]. The interplay of these nonlinear effects broadens the pulse spectrum, promotes self-compression [4] and may lead to the well-known self-guiding of intense light waves over long (meter-range) distances [5]. Filamentation of pulses composed of more than one carrier frequency has moreover been proposed as an innovative way to downconvert optical radiation into the THz range [6] and create broadband THz sources remotely [7].

Interest in terahertz (THz) radiation is motivated by its numerous applications in the fields of physics, chemistry, biology and engineering. Since the advent of ultrafast light sources, laser-induced plasmas have been one of the most promising means to provide ultrabroadband, intense THz waves. However, water vapor considerably attenuates THz wave propagation in air, which limits the efficiency for atmospheric remote sensing. A current challenge for air THz photonics is thus to overcome the strong absorption caused by humidity over meter-range distances. Therefore, the demand for intense THz radiation sources, able to deliver electric fields reaching the GV/m level, is in constant increase. An important constraint

for absorption spectroscopy is also to have broadband spectra in order to measure as many spectral signatures as possible [8].

An efficient method to generate intense and broadband THz radiations consists in focusing two-color ultrashort infrared light pulses composed of fundamental and second harmonic frequencies into the air. If the laser intensity exceeds the medium ionization threshold $\sim 10^{13-14}\,\mathrm{W\,cm^{-2}}$, an electron plasma is created and behaves like a nonlinear frequency converter that produces, through photocurrents, low-frequency emissions belonging to the THz domain [9–11]. Operated in the filamentation regime, extended two-color plasma channels can help produce THz pulses remotely [12], offering a way to overcome water absorption in air. Because THz radiation is also emitted by optical rectification through four-wave mixing [13], Kerr self-focusing may contribute to the overall THz yield [14, 15]. At clamping intensities $> 50\ \mathrm{TW/cm^2}$ from which Kerr self-focusing is stopped by plasma defocusing, THz emission is, nonetheless, dominated by photocurrents and a peak in the THz frequency range appears in the pulse spectrum.

Several techniques exist to increase the THz yield by photocurrents, such as using longer FH wavelengths [16, 17], increasing the number of colors [18, 19] or even modifying the polarization state of the FH and SH components [20, 21]. In this respect, Ref. [21] experimentally evidenced from helium gas jets that circularly polarized two-color pulses with same helicity (CP-S) could deliver ~ 5 times higher THz powers than their linearly polarized, parallel (LP-P) counterparts. This increase in the THz power was attributed in [22] to a direct dependency of the drift velocity acquired by photo-ionized electrons on the dominant FH pump amplitude and longer ionization sequences.

Several important issues in the underlying physics still need to be addressed, such as the role of the Raman-delayed part of the Kerr nonlinearity, which arises due to the excitation of transitions in the molecular constituents of air [23]. To our knowledge, there is no formulation for such Raman-delayed response suitable for laser pulses with arbitrary polarization. Stimulated rotational Raman scattering (SRRS) of a laser pulse in air is a quantum mechanical process involving the excitation of the rotational states of air molecules by the laser pulse [24]. It can be characterized as an instability that scatters laser energy into multiple Stokes and anti-Stokes frequency bands which, because of the dispersive properties of air, propagate at different velocities and at large angles with respect to the input beam, causing a severe distortion of the laser envelope [25].

The present paper aims at clarifying the impact of the Kerr nonlinearities, instantaneous and delayed, on the filament dynamics for two-color pump pulses being either linearly or circularly polarized as well as on THz pulse generation. After deriving the expression of the complete nonlinear polarization for vectorial laser fields, we display numerical evidence that SRRS decreases the THz generation process over long propagation distances [26], even in filamentation regimes where the photocurrent mechanism is the dominating THz emitter. Compared with LP-P pulses, CP-S pulses are found to drive an efficient THz gain over meter distances after the onset of self-focusing while keeping lower clamping intensity and plasma density in the presence of SRRS. These results are confirmed by direct simulations employing the unidirectional pulse propagation equation (UPPE) [27] and they are justified by means of the local current (LC) model [28].

The paper is organized as follows: Section 2 specifies the input laser-gas parameters under consideration and recalls the vectorial model integrated by our unidirectional solver. This section also presents the derivation for the nonlinear Raman response of air molecules based on a microscopic approach. Section 3 addresses our numerical results and discusses the role of SRRS in laser filamentation for linearly or circularly polarized pulses in the presence of a vectorial Raman-delayed nonlinearity. The changes in the laser-to-terahertz efficiency generated by photocurrents versus the optical nonlinearities for different pump pulse polarizations are justified through LC evaluations.

2 The nonlinear responses

We consider two-color input Gaussian pulses with elliptical polarization composed of fundamental (FH, ω_0) and second harmonic (SH, $2\omega_0$),

$$\vec{E}_L(t) = E_0 \exp\left[-2\ln 2\frac{t^2}{\tau_0^2} - \frac{x^2+y^2}{w_0^2}\right] \qquad (1)$$

$$\times \begin{pmatrix} \frac{\sqrt{1-r}}{\sqrt{1+\rho^2}}\sin(\omega_0 t) + \frac{\sqrt{r}}{\sqrt{1+\rho^2}}\sin(2\omega_0 t+\phi) \\ -\frac{\rho\sqrt{1-r}}{\sqrt{1+\rho^2}}\cos(\omega_0 t) - \frac{\rho\sqrt{r}}{\sqrt{1+\rho^2}}\cos(2\omega_0 t+\phi) \end{pmatrix},$$

with FWHM pulse duration $\tau_0 = 50$ fs, spatial width $w_0 = 0.5$ mm, FH wavelength $\lambda_0 = 2\pi c/\omega_0 = 1.6\,\mu$m; $r \simeq 0.2$ denotes the fraction of second harmonic, ϕ is the phase difference between the two colors and ρ is the ellipticity comprised between 0 and 1. When $\rho = 0$, the laser is linearly polarized with both components parallel (LP-P); when $\rho = 1$ the pump is circularly polarized with same helicity in both colors (CP-S) [21].

To understand the effect of the pump polarization onto laser filaments, we review the nonlinear source terms of the medium. It is well-known that femtosecond filaments proceed from local balances between Kerr self-focusing and defocusing due to a tenuous self-generated electron plasma. The plasma response of weakly ionized gases with neutral density N_a is classically modeled by the free electron rate equation

$$\partial_t N_e = W(E)(N_a - N_e), \tag{2}$$

where N_e denotes the electron density, $W(E)$ is the ionization rate depending on the modulus of the vectorial electric field. Triggering sufficient ionization requires high enough intensity, typically larger than 50-100 TW/cm^2, fostering thus the tunnel ionization regime. This rate is ussually given by the instantaneous rate from Ammosov-Delone-Krainov (ADK) theory [10, 29] that reduces for hydrogenoid atoms to the well-known quasi-static tunneling (QST) rate [30]:

$$W(E) = \frac{4(U_i U_H^{-1})^{5/2}\nu_{\rm au}}{|E(t)E_{\rm au}^{-1}|} e^{-\frac{2}{3}\frac{(U_i U_H^{-1})^{3/2}}{|E(t)E_{\rm au}^{-1}|}}, \tag{3}$$

where $U_H = 13.6$ eV denotes the ionization potential of hydrogen; $E_{\rm au} = 514$ GV/m and $\nu_{\rm au} = 41.3$ PHz. Here, we assume that only oxygen is ionized starting from the neutral density $N_a = 5.4\times10^{18}$ cm^{-3} (20% of air compounds) and having the lowest ionization potential $U_i = 12.1$ eV. At moderate intensities $< 10^{15}$ W/cm^2, the electron current density $\vec{J}$ is given by the cold-plasma kinetic equation [9]:

$$\partial_t \vec{J} + \nu_c \vec{J} = \frac{e^2}{m_e} N_e \vec{E}, \tag{4}$$

where e and m_e are the electron charge and mass, respectively, and $\nu_c = 2.85$ ps^{-1} denotes the electron-neutral collision rate.

The optical polarization vector contains linear ($\vec{P}_{\rm L}$) and nonlinear ($\vec{P}_{\rm NL}$) contributions. The Fourier transform of $\vec{P}_{\rm L}$ involves the first-order frequency-dependent susceptibility $\chi^{(1)}(\omega)$ entering the optical linear index $n(\omega) = [1+\chi^{(1)}(\omega)]^{1/2}$. For centro-symmetric media, $\vec{P}_{\rm NL}$ involves the third-order susceptibility $\chi^{(3)}$ responsible for four-wave mixing. For molecular gases, the Kerr response admits a fraction x_K of delayed contribution due to Raman scattering by rotational molecular transitions. Because the laser is not resonant with the transition frequencies [23], SRRS affects the total time-dependent refraction index of the medium through a delayed-Kerr nonlinearity. The instantaneous Kerr nonlinearity $\vec{P}_{\rm inst}(t) = \epsilon_0\chi^{(3)}E^2(t)\vec{E}(t)$, where ϵ_0 is the permittivity in vacuum, is associated with self-phase modulation and nonlinear self-focusing. SRRS, by contrast, leads to the generation of multiple Stokes and anti-Stokes waves that scatter the laser energy. Along this process, a portion of the laser energy is absorbed to excite ro-vibrational transitions of atmospheric molecules, mainly dinitrogen.

In the following we generalized the derivation proposed in [23, 31] to the case of a vector laser pulse. Details can be found in appendix A. Our expression of SRRS for vectorial pulses reads as

$$\vec{P}_R(t) = \epsilon_0\chi^{(3)}\frac{x_K}{2}\int_0^{+\infty} R(\tau)\vec{F}(\vec{E})\,d\tau\,, \tag{5}$$

$$\vec{F}(\vec{E}) = \begin{pmatrix} [3E_x^2(t-\tau)+E_y^2(t-\tau)]E_x(t) \\ [3E_y^2(t-\tau)+E_x^2(t-\tau)]E_y(t) \end{pmatrix}, \tag{6}$$

where $0 \le x_K \le 1$ denotes the SRRS fraction with respect to the instantaneous Kerr response and $R(\tau)$ is the delayed response function

$$R(\tau) = \sin\left(\frac{\tau}{\tau_1}\right)\frac{\tau_1^2+\tau_2^2}{\tau_1\tau_2^2}e^{-\frac{\tau}{\tau_2}}. \tag{7}$$

Here, τ_1 and τ_2 represent the rotational Raman and dipole dephasing times, respectively. In air those quantities take the values $\tau_1 \approx 62.5$ fs and $\tau_2 \approx 77$ fs [23, 32]. The overall nonlinear

polarization thus expresses as

$$\vec{P}_{\rm NL}(t) = \epsilon_0\chi^{(3)}\Big[(1-x_K)E^2(t)\vec{E}(t) + \frac{x_K}{2}\int_0^{+\infty} R(\tau)\vec{F}(\vec{E})\,d\tau\Big]. \quad (8)$$

In our UPPE code, the Raman polarization is recast as

$$\vec{P}_R(t) = \epsilon_0\chi^{(3)}\frac{x_K}{2}\frac{\tau_1^2+\tau_2^2}{\tau_1^2\tau_2^2}\begin{pmatrix}(3Q_x+Q_y)E_x\\(3Q_y+Q_x)E_y\end{pmatrix}, \quad (9)$$

with Q_x and Q_y satisfy the differential equations

$$\frac{d^2Q_x}{dt^2}+\frac{2}{\tau_2}\frac{dQ_x}{dt}+\frac{\tau_1^2+\tau_2^2}{\tau_1^2\tau_2^2}Q_x = E_x^2(t)\,, \quad (10)$$

$$\frac{d^2Q_y}{dt^2}+\frac{2}{\tau_2}\frac{dQ_y}{dt}+\frac{\tau_1^2+\tau_2^2}{\tau_1^2\tau_2^2}Q_y = E_y^2(t)\,. \quad (11)$$

Note that the temporal variations of the second members E_x^2 and E_y^2 are much faster than those caused by the natural frequency of the equations, because $\omega_0 \gg 2\pi/\tau_1$. Therefore, the fast oscillations of the laser field are averaged out during a period of slow variation of Q_x and Q_y. The Raman polarization is thus expected to be mainly high-frequency, and in particular barely contributing to the THz part of the spectrum.

3 UPPE Simulations

We perform $(3+1)$-dimensional numerical computations based on a vectorial version of the unidirectional pulse propagation equation (UPPE) that governs the forward-propagating transverse electric field components E_x, E_y of elliptically polarized pulses. Following [27, 33], our nonlinear propagation model reads as (see also [22])

$$\partial_z\hat{\vec{E}} = {\rm i}\sqrt{k^2(\omega)-k_\perp^2}\,\hat{\vec{E}} + {\rm i}\frac{\mu_0\omega^2}{2k(\omega)}\hat{\vec{\mathcal{F}}}^{\rm NL}\,, \quad (12)$$

where $\hat{\vec{E}}(k_x,k_y,z,\omega)$ is the Fourier transform of the transverse laser electric field components with respect to x, y, and t, and $k_\perp = \sqrt{k_x^2+k_y^2}$. The first term on the right-hand side of Eq. (12) describes linear dispersion and diffraction of the pulse. The term

$$\hat{\vec{\mathcal{F}}}^{\rm NL} = \hat{\vec{P}}_{\rm NL} + {\rm i}\hat{\vec{J}}/\omega + {\rm i}\hat{\vec{J}}_{\rm loss}/\omega$$

contains the third-order nonlinear polarization $\vec{P}_{\rm NL}$ given by Eq. (8) with Kerr index $n_2 \simeq 3\chi^{(3)}/4c\epsilon_0$, the electron current $\vec{J}$ following Eq. (4), and a loss term $\vec{J}_{\rm loss} = [W(E)(N_a - N_e)U_i/E^2]\vec{E}$ due to ionization [2, 4, 22].

Simulations of two-color laser filaments have been performed employing LP-P or CP-S pump pulses, with or without Raman-delayed nonlinear polarization. Our input laser pulses are given by Eq. (1), with an initial phase difference $\phi = \pi$. Dispersion of air is accounted for by the refractive optical index $n(\omega)$ taken from [34]. With $n_2 = 3.8\times10^{-19}$ cm^2/W [35], the critical power for self-focusing, defined by $P_{\rm cr} \simeq \lambda_0^2/2\pi n_2$, is $P_{\rm cr} = 10.7$ GW at 1.6 μm. With 4.43 mJ pulse energy, our beam thus contains 15.5 critical powers. As shown in [12], purely (unperturbed) Gaussian pulses do not directly decay into multiple filaments even for input powers much larger than critical. When SRRS is taken into account, we apply the fraction $x_K \simeq 0.8$ as measured in [35]. The radiated field operating in the THz domain is extracted from a frequency window with cut-off frequency $\nu_{co} = 90$ THz. Our simulations use a time window of 0.8 ps (1.25 THz spectral resolution) and a transverse numerical box of 3×3 mm^2. The numerical resolution steps are $\Delta t = 98$ attoseconds in time and $\Delta x = \Delta y = 12$ μm in transverse space. Such a large spatial step is acceptable at 1.6 μm as the filament width increases like λ_0, and the plasma channel width like $\sqrt{\lambda_0}$ [25]. The maximum laser intensity has input value $I_0 \approx 30$ TW/cm^2 in LP-P configuration and $I_0 \approx 20$ TW/cm^2 in CP-S.

3.1 Results

Figure 1(a) illustrates the peak electron density reached along meter-range distances in two-color filamentation regime for LP-P (blue curves) or CP-S (red curves) polarization whenever an instantaneous nonlinearity only ($x_K = 0$, dashed curves) or the Raman-delayed nonlinearity ($x_K = 0.8$, solid curves) is included. With a purely instantaneous nonlinearity, laser filaments self-focus at about $z_c \approx 10$ cm where they reach ~ 150 TW/cm^2 clamping intensity before relaxing to

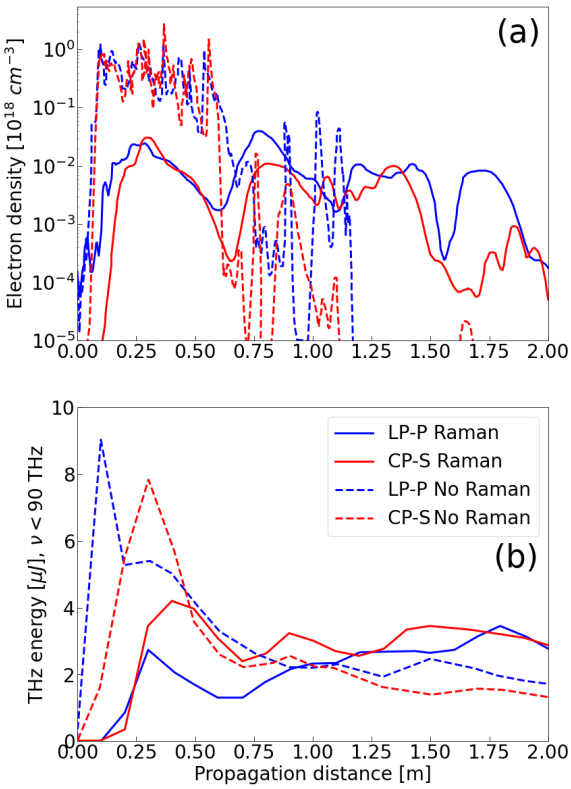

Fig. 1 (a) Peak electron density without SRRS ($x_K = 0$) (dashed curves) and with SRRS ($x_K = 0.8$) (solid curves) for two-color Gaussian pulses in linear polarization (blue curves) or in circular polarization (red curves). (b) Corresponding THz energy in the numerical box (see text).

$\sim 50-100$ TW/cm^2 from $z \geq 50$ cm (not shown). With SRRS, the self-focusing distance is delayed to $z_c \simeq 25-30$ cm from which the clamping intensity does not exceed $50-60$ TW/cm^2. The electron yield follows the same tendency as shown by Fig. 1(a) and exhibits comparable dynamics for both polarization states along the filament range. From this figure it is clear that SRRS, by weakening the contribution of the instantaneous Kerr response, results in a longer self-focusing distance and an enhanced self-guiding range.

Figure 1(b) details the THz energy yield. SRRS, by promoting lower plasma densities, preserves better the laser energy. LP-P pulses undergo the strongest losses through photoionization. Without SRRS (dashed curves), due to a sharp ionization stage in early propagation, the LP-P pulse produces the larger THz energy, which is later followed by a high THz burst promoted by the CP-S pulse as the latter reaches similar ionization levels. Note that the THz energy can escape early our numerical box, which explains why the THz energy curves drop at larger propagation distances. With a smoother self-focusing response due to SRRS (solid curves), the expected hierarchy CP-S > LP-P in terms of THz gains [21, 22] is clearly refound over the first meter of filamentation. We thus confirm the superiority in the THz yield, by a factor close to 2, in the filamentation regime when using circularly polarized pulses compared to linearly polarized ones in realistic air accounting for SRRS, up to fluctuations in the peak electron density at the end of the filament range.

Figure 2 depicts the evolution of the optical and THz spectra along the filamentary propagation. With no SRRS, supercontinuum generation through which all optical frequencies merge to form a plateau of harmonics starts around $z = 10$ cm and is achieved 40 cm further. For comparison, a similar plateau is formed with SRRS from $z > 180$ cm. One can also observe that SRRS tends to inhibit the growth of high-order harmonics in circular polarization. By contrast, THz emission triggered by CP-S pulses takes over that produced with LP-P pulses from $z \geq 50$ cm, in agreement with Fig. 1(bottom).

Finally Fig. 3 displays some temporal profiles of laser fields undergoing plasma-induced distortions along propagation. Typically, the absence of SRRS favors sharper defocusing of the trailing edge of the pulse.

3.2 LC estimates

To understand the above THz gain performances, we can use the Local Current (LC) model [22, 28], based on the approximation that the nonlinear currents are produced locally, ignoring thus propagation effects. According to [36] the radiated field is then proportional to

$$\vec{E}_{\rm rad} \propto \left(\frac{\partial \vec{J}}{\partial t} + \frac{\partial^2 \vec{P}_{\rm NL}}{\partial t^2} \right) . \qquad (13)$$

In order to quantify the suitability of a laser pulse to produce terahertz radiation, we estimate the

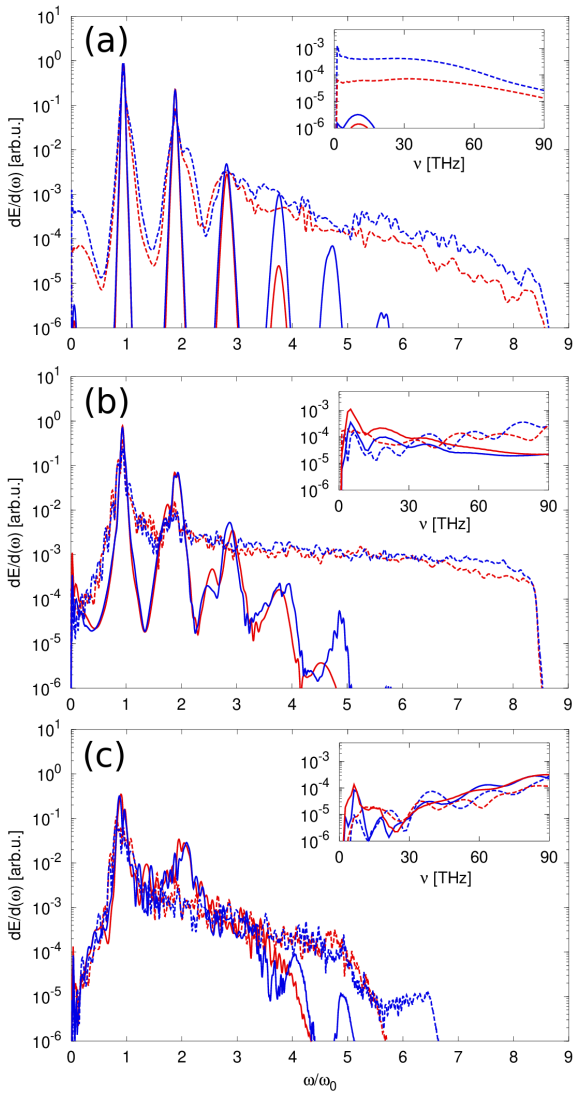

Fig. 2 Optical spectra with THz spectra as insets along different propagation distances: (a) $z = 10$ cm, (b) $z = 50$ cm and (c) $z = 2$ m. Blue (red) curves refer to LP-P (resp. CP-S) pulses. Solid (dashed) refer to accounting for (resp. discarding) SRRS.

terahertz energy yield as

$$\eta_{\mathrm{THz}} = \int_{-\infty}^{+\infty} E_{\mathrm{THz}}^2(t)\, dt\,, \qquad (14)$$

where E_{THz} is the radiated field taken in the THz frequency window $\nu < \nu_{co} = 90$ THz.

Figure 4(a) illustrates the LC contribution of the current density $\vec{J}$ (thus photocurrents) to the THz yield at constant ionization level versus the pump ellipticity ρ, cf. Eq. (1). The most efficient

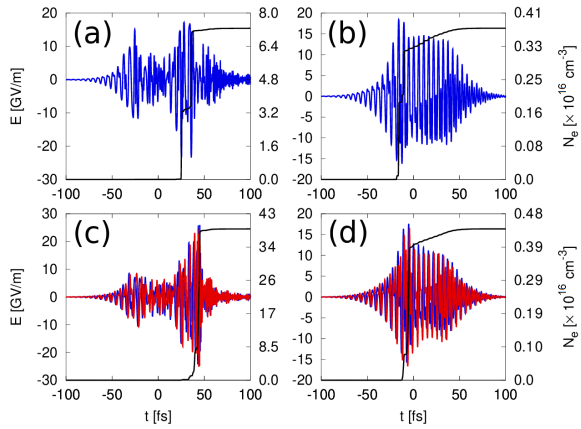

Fig. 3 Optical electric fields E_x (blue curves, left-hand side axis) and E_y (red curves, left-hand side axis) with corresponding density profiles (black curves, right-hand side axis) along time at $z = 50$ cm for (a,b) LP-P and (c,d) CP-S pulses: (a,c) without and (b,d) with Raman effect.

polarization configuration is, as expected, that corresponding to CP-S pulses ($\rho = 1$). For comparison Fig. 4(b) shows the LC contribution of the nonlinear polarization $\vec{P}_{\mathrm{NL}}$ when the Raman response Eq. (5) is taken into account or not. As expected (see also [26]), the influence of the nonlinear polarization (and SRRS) on the THz energy yield is negligible, whatever the pulse polarization may be. Its only relevant role remains in strongly modifying the filamentation dynamics and related spectral evolution through which THz pulse generation may be kept efficient over longer propagation distances.

4 Conclusion

In summary we have derived an expression for the stimulated rotational Raman scattering applied to elliptical (vectorial) laser pulses. The main influence of SRRS is to retard the occurrence of self-focusing and thereby plasma generation. With circularly polarized pulses, plasma is shifted to larger z distances compared with linearly polarized pumps, as circular polarisation promotes lower maximum laser fields (by a factor $1/\sqrt{2}$).

The present work evaluates the efficiency of linear and circular polarization in the generation of THz radiation along the filamentation regime for a realistic air response taking SRRS into account. It appears that, although the THz

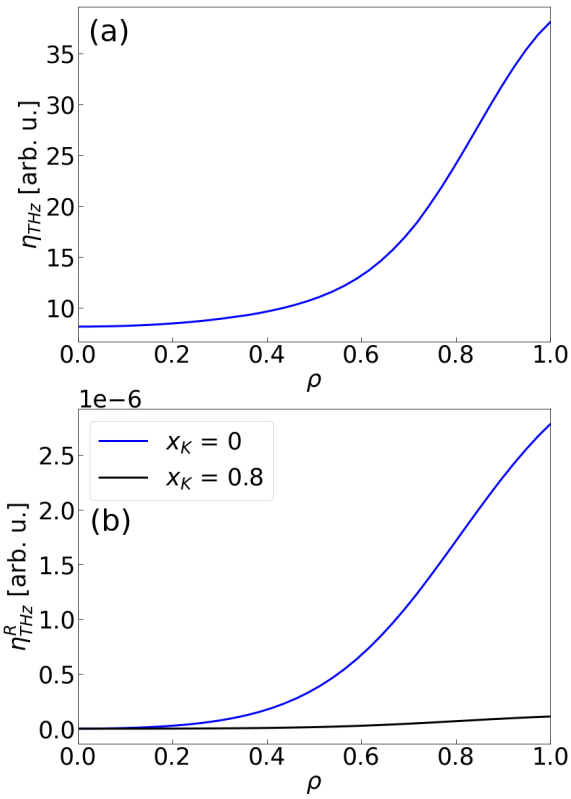

Fig. 4 THz energy yields as function of ρ computed from the LC approach Eqs. (13) and (14) for (a) the photocurrent source and (b) the nonlinear optical response with a purely instantaneous Kerr nonlinearity ($x_K = 0$, blue curve) and with the Raman-delayed Kerr effect ($x_K = 0.8$, black curve). Note the six-order-of magnitude difference between the yields in (a) and (b). The two-color laser field is characterized by $r = 0.2$, $\phi = \pi$ and 100 TW/cm^2 intensity for $\rho = 0$. With increasing ρ, the intensity is adjusted such that the ionization yield remains constant.

energy yield delivered by laser filaments is lowered by Raman scattering in air, the longer filament range reached by smoothing the entire Kerr response allows an efficient THz wave generation over longer propagation ranges. Our simulations demonstrate that THz wave generation in filamentation regime is still reinforced by the use of circularly polarized pulses that promote distortions in the pulse spectrum to the benefit of the THz bandwidth.

5 Appendix

5.1 The microscopic Raman response

Here we derive the nonlinear polarization vector due to Raman scattering in air molecules, assumed to be only due to the rotations of non-interacting dinitrogen molecules. We shall suppose that N_2 molecules have only three energy levels W_1, W_2 and W_3. The first two levels are rotational states attainable by Stockes scattering, and the third is a virtual level of energy much higher than the other two, such that it cannot be directly excited by the laser, i.e., $W_3 \gg W_2 - W_1$. We note also Ω_1, Ω_2 and Ω_3 the respective natural frequencies of these states and $\Omega_{nm} = \Omega_n - \Omega_m$. In view of the above hypotheses, one has $\Omega_{21} \ll \omega_0 \ll \Omega_{32}$.

Let us define $\psi(t, \vec{r})$ the molecular wave function of dinitrogen. We also note H_0 the unperturbed Hamiltonian and $V(t, \vec{r}) = -\vec{\mu} \cdot \vec{E} = -\mu_x E_x - \mu_y E_y = V_x + V_y$ the perturbation operator of the Hamiltonian, with $\vec{\mu} = -e\vec{r}$ the dipole moment vector of N_2 molecules. The Schrödinger equation is therefore written:

$$(H_0 + V_x + V_y)\psi = i\hbar \frac{\partial \psi}{\partial t}. \tag{15}$$

The molecular wave function ψ is decomposed into the sum of eigenstates of H_0, $u_n(\vec{r})$, n being an integer between 1 and 3, $\hbar\Omega_n$ their associated eigenvalues, and $\langle u_m | u_n \rangle = \delta_{mn}$, with δ_{mn} being the Kronecker symbol. Following [23], we substitute

$$\psi(t, \vec{r}) = \sum_{n=1}^{3} c_n(t) e^{-i\Omega_n t} u_n(\vec{r}) \tag{16}$$

into Eq. (15) and treat separately each of its contributions defining $(\vec{\mu} \cdot \vec{E})_{mn} \equiv \mu^x_{mn} E_x + \mu^y_{mn} E_y$ with $\mu^{x,y}_{mn} = \langle u_m | \mu_{x,y} | u_n \rangle$. The time dependent coefficients c_n must then satisfy

$$\frac{\partial c_m(t)}{\partial t} = \frac{i}{\hbar} \sum_{n=1}^{3} c_n(t) (\vec{\mu} \cdot \vec{E})_{mn} e^{-i\Omega_{nm} t}. \tag{17}$$

The microscopic polarization vector $\vec{p}$ is defined as

$$\begin{aligned}\vec{p}(t) &= \langle\psi|\vec{\mu}|\psi\rangle \\ &= \sum_{m=1}^{3}\sum_{n=1}^{3}\rho_{nm}e^{i\Omega_{mn}t}\begin{pmatrix}\mu_{mn}^{x}\\ \mu_{mn}^{y}\end{pmatrix},\end{aligned} \tag{18}$$

with $\rho_{mn} = c_m c_n^*$. By noticing that $\rho_{nm}^* = \rho_{mn}$, $\mu_{mn}^{x,y} = (\mu_{nm}^{x,y})^*$ and $(\vec{\mu}\cdot\vec{E})_{mn} = (\vec{\mu}\cdot\vec{E})_{nm}^*$, one gets

$$\begin{aligned}\frac{\partial\rho_{nm}}{\partial t} = \frac{i}{\hbar}\sum_{j=1}^{3}\Big[&\rho_{jm}(\vec{\mu}\cdot\vec{E})_{nj}e^{-i\Omega_{jn}t} \\ &-\rho_{nj}(\vec{\mu}\cdot\vec{E})_{jm}e^{-i\Omega_{mj}t}\Big].\end{aligned} \tag{19}$$

Similar assumptions as in [23], among which $\rho_{33} = \mu_{12}^{x,y} = \mu_{ii}^{x,y} = 0$ $(1 \le i \le 3)$, give that the non-zero μ_{mn}^{x} (resp. μ_{mn}^{y}) are all equal and assimilate all the coefficients $(\vec{\mu}\cdot\vec{E})_{mn}$ to $(\vec{\mu}\cdot\vec{E})$.

Let us now calculate the elements participating in the macroscopic dipole moment. By using the relation Eq. (18), we obtain

$$\vec{p}(t) = (\rho_{13}e^{i\Omega_{31}t} + \rho_{32}e^{-i\Omega_{32}t})\vec{\mu} + c.c. \tag{20}$$

where ρ_{13} and ρ_{32} are governed by Eq. (19).
To integrate the two equations for ρ_{13} and ρ_{32}, we neglect the time variations of ρ_{11}, ρ_{12}, ρ_{21} and ρ_{22} compared to those of ρ_{13} and ρ_{32}, because $\Omega_{31} \gg \Omega_{21}$ and $\Omega_{31} \sim \Omega_{32}$. With initially $\rho_{13}(t=0) = \rho_{32}(t=0) = 0$, this integration results in

$$\rho_{13}(t) = \frac{(\vec{\mu}\cdot\vec{E})}{\hbar\Omega_{31}}\left(\rho_{11}e^{-i\Omega_{31}t} + \rho_{12}e^{-i\Omega_{32}t}\right), \tag{21}$$

$$\rho_{32}(t) = \frac{(\vec{\mu}\cdot\vec{E})}{\hbar\Omega_{31}}\left(\rho_{12}e^{i\Omega_{31}t} + \rho_{22}e^{i\Omega_{32}t}\right). \tag{22}$$

Since $\rho_{11} + \rho_{22} \simeq 1$ and state 2 remains sparsely populated compared to state 1, we can also assume $\rho_{11} - \rho_{22} \simeq 1$. ρ_{12} is thus given by Eq. (19) as

$$\frac{\partial\rho_{12}}{\partial t} = -\frac{i(\vec{\mu}\cdot\vec{E})^2}{\hbar^2\Omega_{31}}e^{-i\Omega_{21}t}. \tag{23}$$

Following [23], we add an heuristic population decrease of ρ_{12}, related to a decay term with lifetime τ_2. Introducing $\tau_1 = \Omega_{21}^{-1}$, we get

$$\frac{\partial\rho_{12}}{\partial t} = -\frac{\rho_{12}}{\tau_2} - \frac{i(\vec{\mu}\cdot\vec{E})^2}{\hbar^2\Omega_{31}}e^{-i\frac{t}{\tau_1}}. \tag{24}$$

Using these expressions, we can simplify the expression for the nonlinear part of the polarization vector oriented along $\hat{\mu} = \vec{\mu}/\mu$ to

$$\vec{p}_R(t) = \frac{2\mu^2}{\hbar\Omega_{31}}(\hat{\mu}\cdot\vec{E})\rho_{12}e^{i\Omega_{21}t}\hat{\mu} + c.c., \tag{25}$$

and finally obtain after solving Eq. (24)

$$\begin{aligned}\vec{p}_R(t) = \frac{1}{\hbar}\left(\frac{2\mu^2}{\hbar\Omega_{31}}\right)^2[\hat{\mu}\cdot\vec{E}(t)] \\ \times\int_{-\infty}^{t}[\hat{\mu}\cdot\vec{E}(t')]^2\sin\left(\frac{t-t'}{\tau_1}\right)e^{\frac{t'-t}{\tau_2}}\,dt'\hat{\mu}.\end{aligned} \tag{26}$$

Finally let ξ be the angle between $\vec{\mu}$ and $\vec{e_x}$. To obtain a macroscopic expression of the Raman polarization, it is necessary to average the above expression over all angles ξ and multiply the expression by the molecular density of the medium N_a. For isotropic air, the angle ξ is distributed uniformly between 0 and 2π. The macroscopic Raman polarization is thus given by

$$\vec{P}_R(t) = \frac{N_a}{2\pi}\int_0^{2\pi}\vec{p}_R(t,\xi)d\xi. \tag{27}$$

After integration we obtain the final form of the Raman polarization Eq. (5) for a vector laser field. Note that if we set $E_y = 0$, we recover the standard one-dimensional expression of [23] for a linearly polarized laser pulse.

Acknowledgments. The authors acknowledge the Agence Nationale de la Recherche (ANR - ALTESSE: ANR-19-ASMA-0007). Numerical simulations were performed using resources at Grand Équipement National De Calcul Intensif (GENCI) (A0100507594). S. Skupin thanks the Qatar National Research Fund (NPRP 12S-0205-190047) for support.

References

[1] Chin, S.L., Hosseini, S.A., Liu, W., Luo, Q., Théberge, F., Aközbek, N., Becker, A., Kandidov, V.P., Kosareva, O.G., Schroeder,

H.: The propagation of powerful femtosecond laser pulses in optical media: Physics, applications, and new challenges. Can. J. Phys. **83**, 863 (2005)

[2] Bergé, L., Skupin, S., Nuter, R., Kasparian, J., Wolf, J.P.: Optical ultrashort filaments in weakly-ionized, optically-transparent media. Rep. Prog. Phys. **70**, 1633 (2007)

[3] Kasparian, J., Wolf, J.-P.: Physics and applications of atmospheric nonlinear optics and filamentation. Opt. Express **16**, 466 (2008)

[4] Bergé, L., Skupin, S.: Few-cycle light bullets created by femtosecond filaments. Phys. Rev. Lett. **100**, 113902 (2008)

[5] Kasparian, J., Rodriguez, M., Méjean, G., Yu, J., Salmon, E., Wille, H., Bourayou, R., Frey, S., André, Y.B., Mysyrowicz, A., Sauerbrey, R., Wolf, J.P., Wöste, L.: White-light filaments for atmospheric analysis. Science **301**, 61 (2003)

[6] Wang, T.-J., Chen, Y., Marceau, C., Théberge, F., Châteauneuf, M., Dubois, J., Chin, S.L.: High energy terahertz emission from two-color laser-induced filamentation in air with pump pulse duration control. Appl. Phys. Lett. **95**, 131108 (2009)

[7] Liu, J., Dai, J., Chin, S.L., Zhang, X.-C.: Broadband terahertz wave remote sensing using coherent manipulation of fluorescence from asymmetrically ionized gases. Nat. Photon. **4**, 627 (2010)

[8] Bergé, L., Kaltenecker, K., Engelbrecht, S., Nguyen, A., Skupin, S., Merlat, L., Fischer, B., Zhou, B., Thiele, I., Jepsen, P.U.: Terahertz spectroscopy from air plasmas created by two-color femtosecond laser pulses: The ALTESSE project. Eur. Phys. Lett. **126**(2), 24001 (2019)

[9] Kim, K.Y., Taylor, A.J., Glownia, J.H., Rodriguez, G.: Coherent control of terahertz supercontinuum generation in ultrafast laser-gas interactions. Nat. Photon. **2**, 605 (2008)

[10] Thomson, M.D., Kress, M., Löffler, T., Roskos, H.G.: Broadband THz emission from gas plasmas induced by femtosecond optical pulses: From fundamentals to applications. Laser Photon.& Rev. **1**, 349 (2007)

[11] Babushkin, I., Kuehn, W., Köhler, C., Skupin, S., Bergé, L., Reimann, K., Woerner, M., Herrmann, J., Elsaesser, T.: Ultrafast spatiotemporal dynamics of terahertz generation by ionizing two-color femtosecond pulses in gases. Phys. Rev. Lett. **105**, 053903 (2010)

[12] Bergé, L., Skupin, S., Köhler, C., Babushkin, I., Herrmann, J.: 3D numerical simulations of THz generation by two-color laser filaments. Phys. Rev. Lett. **110**, 073901 (2013)

[13] Cook, D.J., Hochstrasser, R.M.: Intense terahertz pulses by four-wave rectification in air. Opt. Lett. **25**, 1210 (2000)

[14] Borodin, A.V., Panov, N.A., Kosareva, O.G., Andreeva, V.A., Esaulkov, M.N., Makarov, V.A., Shkurinov, A.P., Chin, S.L., Zhang, X.-C.: Transformation of terahertz spectra emitted from dual-frequency femtosecond pulse interaction in gases. Opt. Lett. **38**, 1906 (2013)

[15] Andreeva, V.A., Kosareva, O.G., Panov, N.A., Shipilo, D.E., Solyankin, P.M., Esaulkov, M.N., González de Alaiza Martínez, P., Shkurinov, A.P., Makarov, V.A., Bergé, L., Chin, S.L.: Ultrabroad terahertz spectrum generation from an air-based filament plasma. Phys. Rev. Lett. **116**, 063902 (2016)

[16] Clerici, M., Peccianti, M., Schmidt, B.E., Caspani, L., Shalaby, M., Giguère, M., Lotti, A., Couairon, A., Légaré, F., Ozaki, T., Faccio, D., Morandotti, R.: Wavelength scaling of terahertz generation by gas ionization. Phys. Rev. Lett. **110**, 253901 (2013)

[17] Nguyen, A., Kaltenecker, K.J., Delagnes, J.-C., Zhou, B., Cormier, E., Fedorov, N., Bouillaud, R., Descamps, D., Thiele, I., Skupin, S., Jepsen, P.U., Bergé, L.: Wavelength scaling of terahertz pulse energies delivered by two-color air plasmas. Opt. Lett. **44**, 1844 (2019)

[18] González de Alaiza Martínez, P., Babushkin, I., Bergé, L., Skupin, S., Cabrera-Granado, E., Köhler, C., Morgner, U., Husakou, A., Herrmann, J.: Boosting terahertz generation in laser-field ionized gases using a sawtooth wave shape. Phys. Rev. Lett. **114**, 183901 (2015)

[19] Vaičaitis, V., Balachninaitė, O., Morgner, U., Babushkin, I.: Terahertz radiation generation by three-color laser pulses in air filament. J. Appl. Phys. **125**, 173103 (2019)

[20] Dai, J., Karpowicz, N., Zhang, X.-C.: Coherent polarization control of terahertz waves generated from two-color laser-induced gas plasma. Phys. Rev. Lett. **103**, 023001 (2009)

[21] Meng, C., Chen, W., Wang, X., Lü, Z., Huang, Y., Liu, J., Zhang, D., Zhao, Z., Yuan, J.: Enhancement of terahertz radiation by using circularly polarized two-color laser fields. Appl. Phys. Lett. **109**, 131105 (2016)

[22] Tailliez, C., Stathopulos, A., Skupin, S., Buožius, D., Babushkin, I., Vaičaitis, V., Bergé, L.: Terahertz pulse generation by two-color laser fields with circular polarization. New J. Phys. **22**, 103038 (2020)

[23] Peñano, J.R., Sprangle, P., Serafim, P., Hafizi, B., Ting, A.: Stimulated raman scattering of intense laser pulses in air. Phys. Rev. E **68**, 056502 (2003)

[24] Boyd, R.W. (ed.): Nonlinear Optics. Academic Press, San Diego (1992)

[25] Champeaux, S., Bergé, L.: Postionization regimes of femtosecond laser pulses self-channeling in air. Phys. Rev. E **71**, 046604 (2005)

[26] Nguyen, A., de Alaiza Martínez, P.G., Déchard, J., Thiele, I., Babushkin, I., Skupin, S., Bergé, L.: Spectral dynamics of thz pulses generated by two-color laser filaments in air: the role of kerr nonlinearities and pump wavelength. Opt. Express **25**, 4720 (2017)

[27] Kolesik, M., Moloney, J.V.: Nonlinear optical pulse propagation simulation: From Maxwell's to unidirectional equations. Phys. Rev. E **70**, 036604 (2004)

[28] Babushkin, I., Skupin, S., Husakou, A., Köhler, C., Cabrera-Granado, E., Bergé, L., Herrmann, J.: Tailoring terahertz radiation by controling tunnel photoionization events in gases. New J. Phys. **13**, 123029 (2011)

[29] Ammosov, M.V., Delone, N.B., Kraĭnov, V.P.: Tunnel ionization of complex atoms and of atomic ions in an alternating electromagnetic field. Sov. Phys. JETP **64**, 1191 (1986)

[30] Landau, L.D., Lifshitz, E.M.: Quantum Mechanics. Pergamon, New-York (1965)

[31] Sprangle, P., Peñano, J.R., Hafizi, B.: Propagation of intense short laser pulses in the atmosphere. Phys. Rev. E **66**, 046418 (2002)

[32] Pitts, T.A., Luk, T.S., Gruetzner, J.K., Nelson, T.R., McPherson, A., Cameron, S.M., Bernstein, A.C.: Propagation of self-focusing laser pulses in atmosphere: experiment versus numerical simulation'. J. Opt. Soc. Am. B **21**, 2008 (2004)

[33] Kolesik, M., Moloney, J.V., Mlejnek, M.: Unidirectional optical pulse propagation equation. Phys. Rev. Lett. **89**, 283902 (2002)

[34] Peck, E.R., Reeder, K.: Dispersion of air. J. Opt. Soc. Am. A **62**, 958 (1972)

[35] Zahedpour, S., Wahlstrand, J.K., Milchberg, H.M.: Measurement of the nonlinear refractive index of air constituents at mid-infrared wavelengths. Opt. Lett. **40**, 5794 (2015)

[36] Jefimenko, O.D.: Electricity and Magnetism: An Introduction to the Theory of Electric and Magnetic Fields. Appleton-Century-Crofts, New York (1966)